Proceedings of the Second International Workshop on EGS, 8.-12. August 2000, Tsukuba, Japan
KEK Proceedings 200-20, pp.316-323

Simulation of Ionization and Scintillation Signals in a Liquid Ionization Drift Chamber

T. Shimoyama, E. Shibamura[1], M. Miyajima

Department of Applied Physics, Fukui University
3-9-1, Bunkyo, Fukui-shi, 910-8507, Japan
[1] *College of Health Science, Saitama Pref. University*
820, San-nomiya, Koshigaya-shi, Saitama-ken, 343-8540, Japan

Abstract

In order to search for double beta-decay events under existence of many background events, We have simulated double beta-decay events of ^{136}Xe in liquid xenon ionization drift chamber by EGS/PRESTA Monte Carlo code to construct data-sets for analyzing the position resolution of vertex point from ionization and scintillation signals, which are observed with collecting charges and scintillation photons generated by two beta-particles in liquid xenon. The ionization drift chamber is a single gridded ionization chamber with a segmented collector of $200 \times 50 \times 42mm^3$ in size.

The position resolutions, which are calculated with the drift time and the position of electron swarms formed by two beta-particles, were $\Delta Y_{0\nu} = 1.501 \pm 0.004mm$ and $\Delta Z_{0\nu} = 0.1249 \pm 0.005$, $\Delta Y_{2\nu} = 0.1231 \pm 0.003mm$ and $\Delta Z_{2\nu} = 0.0747 \pm 0.002mm$, respectively. The same, which are calculated with the number of photoelectrons observed at each photo-multiplier, were $\Delta Y_{0\nu} = 9.92 \pm 0.06mm$ and $\Delta Z_{0\nu} = 8.56 \pm 0.05$, $\Delta Y_{2\nu} = 9.58 \pm 0.05mm$ and $\Delta Z_{2\nu} = 8.44 \pm 0.05mm$, respectively.

1 Introduction

In the double beta decay, there are two main decay channels, $(A, Z) \rightarrow (A, Z+2)+e_1+e_2+\overline{\nu}_{e1}+\overline{\nu}_{e2}$ ($2\beta 2\nu$ mode) and $(A, Z) \rightarrow (A, Z+2) + e_1 + e_2$ ($2\beta 0\nu$ mode). Two-neutrino decay ($2\beta 2\nu$) can be understood by the second order weak intaraction. In neutrinoless decay ($2\beta 0\nu$), a neutrino emitted at single beta decay is absorbed by other nucleon and the nucleon decays by emitting an electron. This decay will be possible if neutrino is massive Majorana neutrino and/or right-handed current exists.[1] Furthermore, this decay violates the law of lepton number coservation. So there must be physics beyond the standard model.

In double beta-decay searches, we can only observe two emitted beta rays at a decay, of which the transition energy is normally low. Therefore, we have to look for double beta-decay events under existence of many background events, which are due to environmental radiation, cosmic rays and so on.

We have proposed a liquid xenon ionization drift chamber equipped with a daughter identification system by laser fluorescence to search for double beta decay events of ^{136}Xe.[2] Liquid xenon will be used for the following several reasons:

1. the W-value of $15.6eV$ [3] is the smallest among liquid inert gases, so we can expect larger signal sizes with a relatively good energy resolution.

2. electrons in liquid xenon moves with relatively large mobility and the drift velocity is almost constant of about $3mm/\mu sec$ under the electric field of $3kV/cm$ or higher[4, 5], so we can expect the ionization chamber will be operated as an drift chamber.

3. the scintillation, which is very fast phenomena, can be used as the trigger signal of events because that is observable with ionization at the same time.[6]

4. the daughter ions of ^{136}Xe are expected to be stable in liquid xenon and move slowly under an electric fields.[7]

The detector previously proposed is a semi-cylindrical gridded ionization chamber. Segmented electrodes fixed at the inside surface of the outermost cylinder collect electrons liberated by two beta rays and determine the sum energy of two beta rays and the position of the decay from the drift time of the electron swarm from the segment position. The daughter ion drifts toward the central electrode and will be observed near the electrode with photo-multiplier tubes fixed above the chamber by the laser fluorescence.

Here, we describe the results of simulation of ionization and scintillation signals on a different type of the liquid xenon ionization drift chamber for comparison to the previous detector. In order to calculate the signal sizes which we can obtain in the detector, we construct data-sets composed of the energy deposition of two beta rays emitted at a double beta decay simulated with EGS/PRESTA code. From two data-sets of which one is for $2\beta 2\nu$ mode and the other is for $2\beta 0\nu$ mode, we calculated distances between the vertex point of a double beta decay and the point determined by the ionization and scintillation signals to estimate the beam size for laser shot. We also calculated detection efficiencies and effective volumes of the detector to the both mode, and energy spectra on a triggering level by observation of scintillation photons.

2 Detector

The detector used in this simulation is a plane parallel liquid xenon single gridded ionization drift chamber equipped with a daughter identification system by laser fluorescence. The schematic drawing is shown in Fig.1 without the daughter identification system. The laser beam to identify daughter ions is shot to a X-direction. The volume of the chamber is $200 \times 50 \times 42 mm^3$. The collector electrode, which collects electron swarms liberated by two beta rays, locates at the bottom and is segmented into 20 strips of $2mm \times 200mm$ with a pitch of $2.5mm$. The Frish grid is an array of gold plated tungsten wires of $100\mu m$ in diameter. The grid is located at $2mm$ above the collector and the wires are strung with a spacing of $1mm$ parallel to Y-direction. The cathode, which collect the daughter ions, situates at $40mm$ above the grid. In order to observe the scintillation (VUV) and fluorescence (visible) photons, two different types of photo-multiplier tube (PMT), of which 10 PMTs of $12.5mm$ in diameter are for VUV photons and 4 PMTs of $50mm$ in diameter are for visible photons, are fixed just above the cathode. The scintillation signals are used to trigger the circuit for drift time measurements and also used to roughly estimate the position of a daughter ion in a double beta decay event. The sum energy of two beta rays is measured with the total ionization yields collected at each segmented electrode. The position of the daughter ion is accurately determined from the distribution of ionization yields on the several segments and the electron drift times.

3 Simulation model

The detector medium is liquid xenon of 100% enriched ^{136}Xe which is the double beta decay source. The density of liquid is $3.06 g/cm^3$ and the total weight $1.24 kg$. The chamber is divided into two volumes, of which one is active and drift space of electron swarms and the other is the dead volume between the collector and the grid. The whole volume of detector is divided into $200 \times 50 \times 42$ cells and the energy deposition due to two beta rays in each cell is simulated by EGS4 code. At each event of the double beta decays, the coordinates of the vertex point, the number of cells in which any energy deposition exists, and an assembly that the position of a cell and the energy deposition into the cell are all memorized into a data-set. The source of double beta decays is uniformly distributed

inside the whole volume. Then, we produced two data-sets of which one is for $2\beta0\nu$ decays and the other is for $2\beta2\nu$ decays.

3.1 $2\beta0\nu$ decay

The sum energy of two beta rays emitted through this mode is equal to the Q-value of $2.479MeV$. Then, one electron with the kinetic energy T_1 in unit of electron mass is generated according to the distribution function of Eq.1[8] and the energy of the other is given by the sum energy of $2.479MeV$. The distribution function of the single electron in $2\beta0\nu$ decay is given by

$$F(T_1) = (T_1 + 1)^2 (T_0 + 1 - T_1)^2, \tag{1}$$

where T_1 is kinetic energy in unit of the electron mass energy, T_0 is Q-value in the same unit. In simulation the two electrons are assumed to emit simply back-to-back.

3.2 $2\beta2\nu$ decay

In $2\beta2\nu$ decay, the distribution function of single electron and the sum energy are given by

$$F_1(T_1) = (T_1 + 1)^2 (T_0 - T_1)^6 \left[(T_0 - T_1)^2 + 8(T_0 - T_1) + 28 \right], \tag{2}$$

$$F(T) = (T^4 + 10T^3 + 40T^2 + 60T + 30) T (T_0 - T)^5, \tag{3}$$

where T_1 is the kinetic energy of single electron, T_0 the Q-value, and T the sum-energy of emitted electrons. T_1, T_0, T are all given in unit of electron mass energy. One electron with kinetic energy of T_1 is generated according to Eq.2 [8] and the other electron is generated to satisfy the distribution function of the sum energy T given by Eq.3. The two electrons are assumed to emit back-to-back.

4 Ionization and Scintillation Signals

In order to get signal sizes from the data-sets mentioned above, the energy deposition in every cell is converted to the number of electrons and photons by using the W-value ($15.6eV$) for ionization and the Ws-value ($16.3eV$) for scintillation. However, the number of photons emitted under the electric field of operation is reduced to almost 1/3. Then, we use an estimated value of $50eV/photon$ to get the number of photons.

4.1 Ionization signals

In order to properly operate the drift chamber, the electric field between the grid and the collector is so kept 2 to 3 times stronger than one between the grid and the cathode that the grid does not capture even a fraction of electron swarms. Therefore, the drift velocity of electrons between the grid and the collector is slightly larger than that between the cathode and the grid. Here, we used drift velocities of $2.1mm/\mu sec$ and $1.9mm/\mu sec$, respectively, to calculate rise times of ionization signals at the collector segments. The total number of electrons collected at the collector was calculated event by event and was again converted to the energy. The total energy deposition in the active volume is shown in Fig.2 in the case of $2\beta0\nu$ decay mode. The spectrum in the case of $2\beta2\nu$ decay events is also shown in Fig.3. The position of an event on Y-direction was determined from the centroid of the charge distribution spread over several collector segments. Then, the distance between the vertex point and the position of events was calculated. The displacement of the position from the vertex point is shown in Fig.4 in the case of $2\beta0\nu$ decay mode. The position of every event on Z-direction was calculated from the drift time when 90% of electrons reached to the collector and the drift time was converted to the distance from the collector. The displacement of the position determined with the drift time from the vertex point is plotted in Fig.5 in the case of $2\beta0\nu$ decay events. In the case of $2\beta2\nu$ decay events, the displacement on Y-direction is shown in Fig.6 and the same on Z-direction is shown in Fig.7.

4.2 Scintillation signals

The VUV sensitive PMT observes scintillation photons. The energy deposition in every cell is converted to the number of photoelectrons at every PMT, using the solid angle subtended by every PMT to every cell and assuming the quantum efficiency of all the PMT is 10%. Since this calculation generates fractional figures in the number of photoelectrons, we obtained its integral number, assuming the fractional photoelectron number shows an expected value in Poisson distribution. The histograms of the displacement on the position determined with the number of photoelectrons at every PMT from the vertex point are shown in Fig.8 to 11 for the both cases of decay modes.

5 Results and Discussions

We can estimate the efficiencies for detection of double beta decay events in the both decay modes. Firstly, we blur the spectrum shown in Fig.1 with fluctuations due to electronic noise of the preamplifier, rise time effect in shaping circuit, shielding inefficiency of the grid and ionization straggling. Assuming the energy resolution is determined from the total width due to those effects, the detection efficiency, which is defined as a ratio of the number of counts detected with the energy interval inside $2 \times FWHM$ at the peak to the total events, is plotted as a function of the energy resolution in Fig.12 in the case of $2\beta0\nu$ decay mode. We expect the detection efficiency of about 84% with a plausible resolution of 3 to 4%. The efficiency in the case of $2\beta2\nu$ decay mode is largely depend on the threshold energy of the detection system and is plotted as a function of threshold in Fig.13. A factor, which determines the threshold energy in $2\beta2\nu$ decay events, is a triggering level determined by the number of photoelectrons. As the level increases, the efficiency decreases as shown in Fig.14.

As our next step, the angular correlation should be incorporated into the simulation of the double beta decays, because we assume two beta rays emit back-to-back in the simulation.

References

[1] M. Doi et al., *Prog. Th. Phys.* **66**(1981)1739; M. Doi et al., *Prog. Th. Phys.* **66**(1981)1765.

[2] M .Miyajima et al., *A I P conf. Proc.* **388**, Resonance Ionization Spectroscopy 253(1996).

[3] T. Takahashi et al., *Phys. Rev.* **12A**(1975)1771.

[4] L. S. Miller, S. Home and W. E. Spear, *Phys. Rev.* **116**(1968)871.

[5] M. Miyajima et al., *IEEE Trans. Nucl. Sci.* **NS39**(1992)536.

[6] S. Kubota et al., *Nucl. Instr. and Meth.* **196**(1982)101.

[7] M. Miyajima et al., Presented at the 55th the meeting of Physical Society of Japan, Sep. 2000.

[8] V. I. Tretyak and YU. G. Zdesenko, *At. Data Nucl. Data Tabl.* **61**(1993)43.

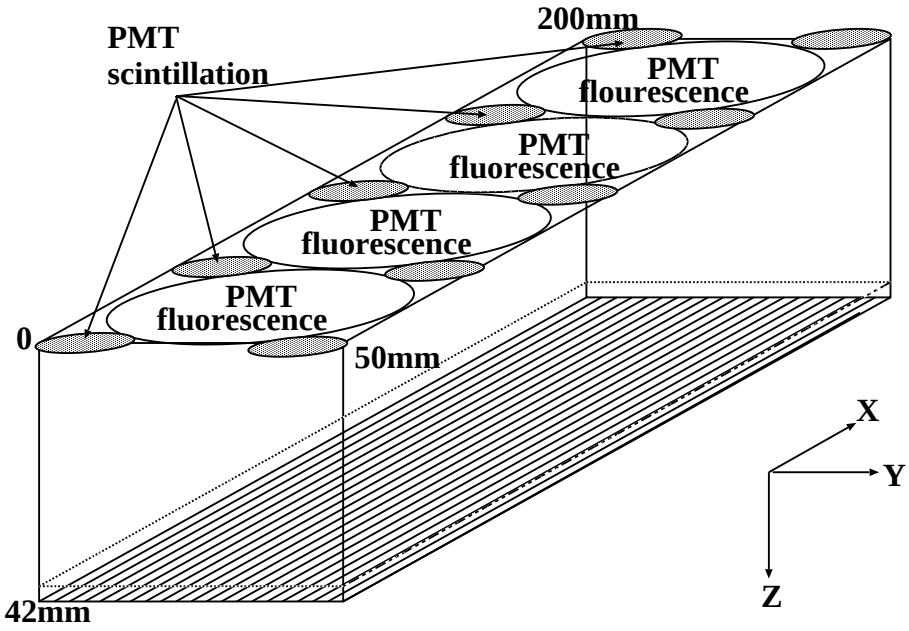

Figure 1: Simulation model for EGS4. Size:$200 \times 50 \times 42 mm^3$, matter:liquid xenon enriched ^{136}Xe (outside: vacuum)

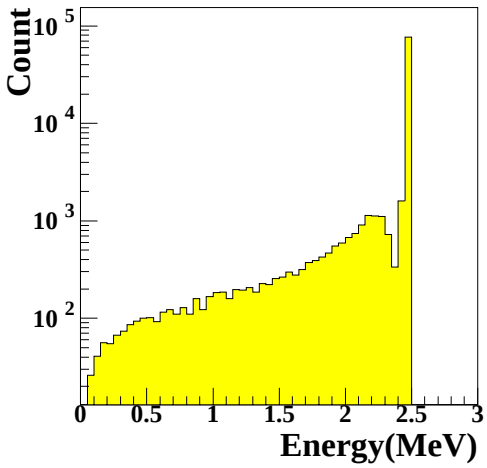

Figure 2: Spectrum of the total energy deposition in the active volume in the case of $2\beta 0\nu$ decay events

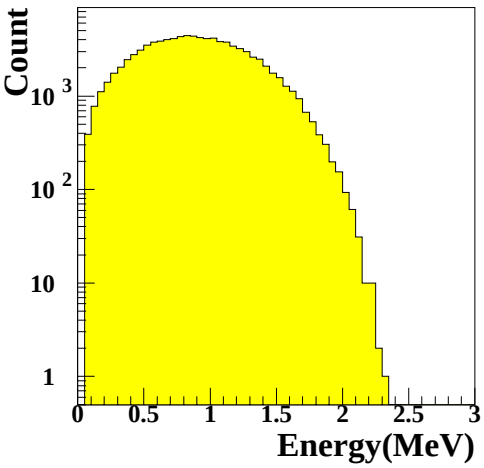

Figure 3: Spectrum of the total energy deposition in the active volume in the case of $2\beta 2\nu$ decay events

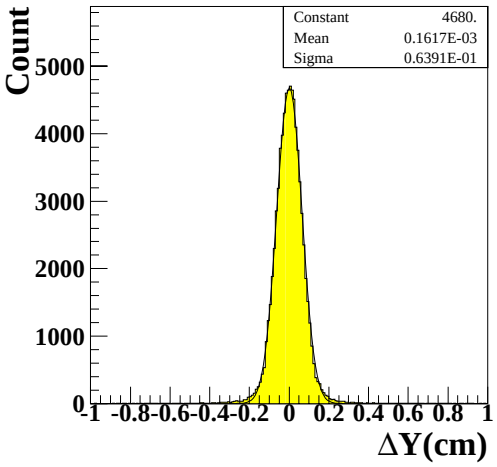

Figure 4: Distribution of the displacement: the position where the double beta decay occurs and the centroid of the charge signals from strips in $2\beta0\nu$ decay

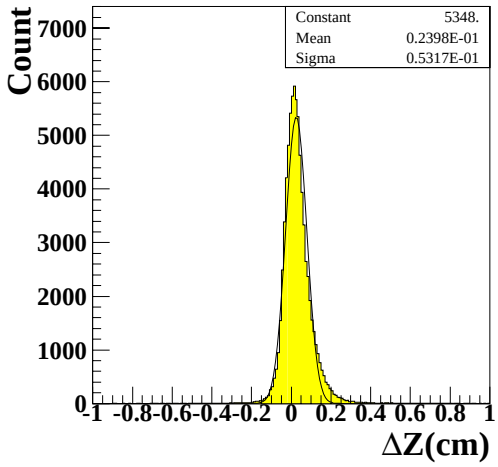

Figure 5: Distribution of the displacement: the position where the double beta decay occurs and the centroid of the charge signals from strips in $2\beta0\nu$ decay

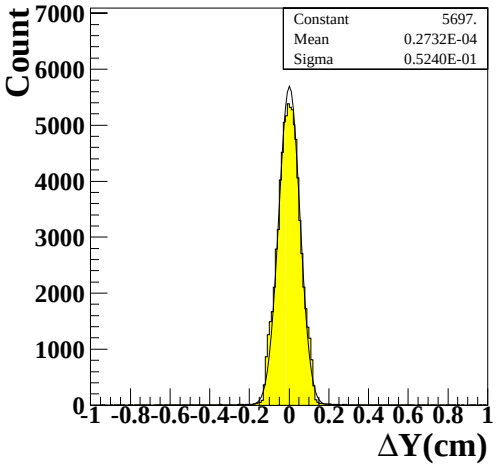

Figure 6: Distribution of the displacement: the position where the double beta decay occurs and the centroid of the charge signals from strips in $2\beta2\nu$ decay

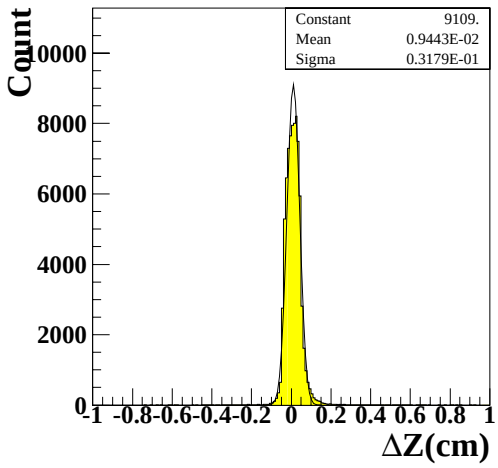

Figure 7: Distribution of the displacement: the position where the double beta decay occurs and the centroid of the charge signals from strips in $2\beta2\nu$ decay

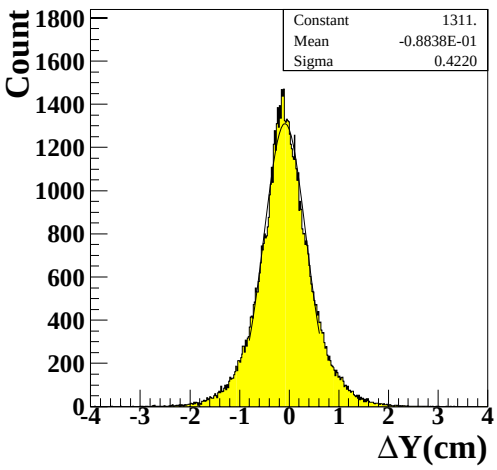

Figure 8: Distribution of the displacement: the position where the double beta decay occurs and the centroid of the signals from PMTs in $2\beta0\nu$ decay

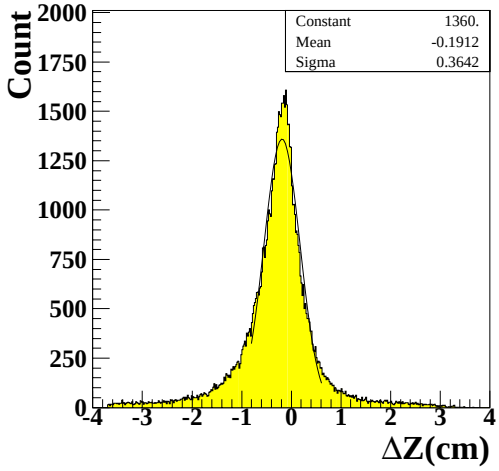

Figure 9: Distribution of the displacement: the position where the double beta decay occurs and the centroid of the signals from PMTs in $2\beta0\nu$ decay

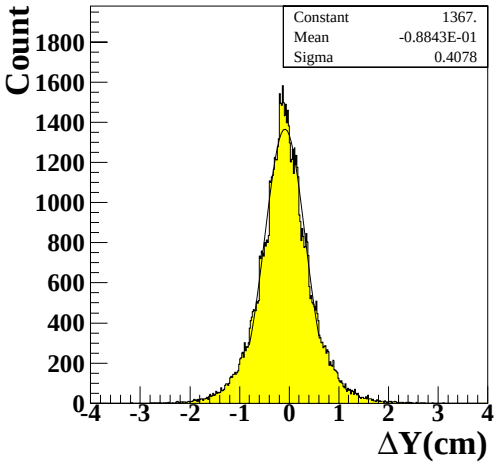

Figure 10: Distribution of the displacement: the position where the double beta decay occurs and the centroid of the signals from PMTs in $2\beta2\nu$ decay

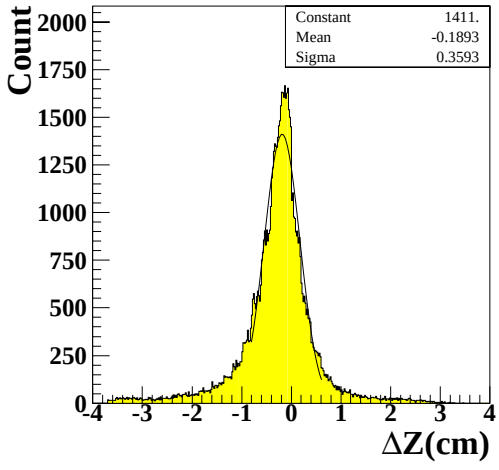

Figure 11: Distribution of the displacement: the position where the double beta decay occurs and the centroid of the signals from PMTs in $2\beta2\nu$ decay

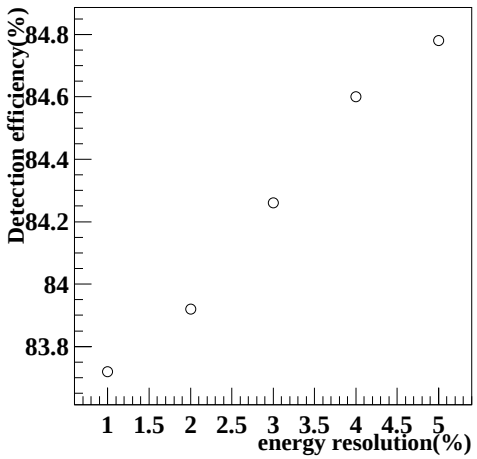

Figure 12: Detection efficiency of $2\beta0\nu$ decay events as a function of energy resolution

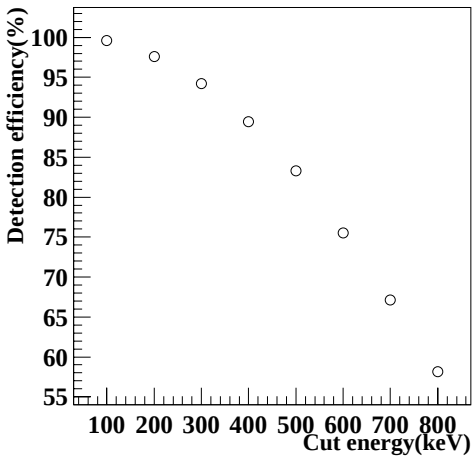

Figure 13: Detection efficiency of $2\beta2\nu$ decay events as a function of threshold energy

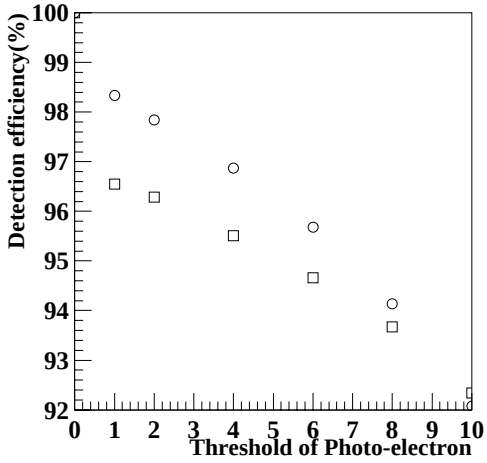

Figure 14: Detection efficiency of two decay modes as a function of triggering level; where ∘ : $2\beta0\nu$ decay mode, □ : $2\beta2\nu$ decay mode